Update on Scroll Compressor Chamber Geometry

I. BELL[1]*, E.A. GROLL[1], J.E. BRAUN[1], G. KING[1]

[1]Purdue University, Department of Mechanical Engineering,
West Lafayette, IN, 47906, USA

* Corresponding Author (e-mail: ibell@purdue.edu)

ABSTRACT

The geometry of the scroll compressor determines the efficiency of the scroll compressor and controls all elements of its operation. It is therefore critical to be able to accurately model the volumes of the compressor over the course of a revolution. This paper proposes a novel quasi-analytic formulation of the suction, compression and discharge chambers based on a change of variables from involute angle to polar integration angle. This solution has been compared against a reference polygon solution, and for the suction chamber this solution agrees to within 0.02%. The solutions for the compression and discharge chamber volumes are analytic and incur a negligible penalty to overhead of a detailed compressor model. In addition, the general nature of the solution presented allows for multiple compression chambers and more complex discharge geometry.

1. INTRODUCTION

Since the scroll compressor was proposed by Creux in 1905, the geometry of the scroll compressor has been the study of a number of researchers. The modern analysis of the geometry of the scroll compressor begins with Yanagisawa (1990) who developed relationships for the geometry of the compressor chambers using an integration of the involute angle for a fixed set of initial angles, and a correction term for the suction chamber. The discharge chamber was treated with a simplified arc clearance volume. This same fundamental analysis method was applied by Halm (1997) and Chen (2002).

The next major breakthrough in the scroll compressor geometry analysis came with Gravesen (2001), who proposed a novel reference frame for the analysis of the scroll compressor geometry, opening the door for the analysis of variable-wall-thickness scrolls. Gravesen's analysis is the cornerstone of the work of Blunier (2006) and Blunier (2009).

Wang (2005) noted the limitation of fixed initial involute angles of the analysis of Halm and Chen, and developed a model which allowed for discretionary initial angles of involute, but still used the approximate correction term to the suction chamber volume from Yanagisawa.

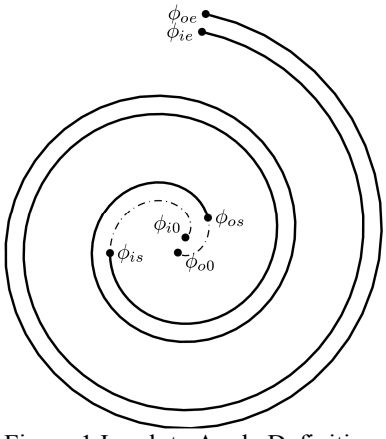

Figure 1 Involute Angle Definitions

2. COMPRESSOR GEOMETRY OVERVIEW

The geometry of the scroll compressor is based on the involute of a circle. **Error! Reference source not found.** shows the geometry of a set of involutes which form the fixed scroll. A small overview of the involute geometry is given here; for more information refer to Yanagisawa (1990), Halm (1997), Chen (2002), Wang (2005), Blunier (2006), Blunier (2009), and Gravesen (2001).

Each of the involutes forming the fixed scroll can be defined by

$$\left(x_f, y_f\right) = \left(r_b\left(\cos\phi + \left(\phi - \phi_0\right)\sin\phi\right), r_b\left(\sin\phi - \left(\phi - \phi_0\right)\cos\phi\right)\right) \tag{1}$$

where ϕ ranges from ϕ_{is} to ϕ_{ie} and ϕ_{os} to ϕ_{oe} for the inner and outer involutes respectively, and the initial angle ϕ_0 is the initial angle of the respective involute (either inner or outer) . The thickness of the scroll wrap can be defined by $t=r_b(\phi_{i0}-\phi_{o0})$. The fixed scroll is mated with an orbiting scroll with the same construction but reflected through the origin and offset by a constant-length vector of length $r_o=r_b(\pi-\phi_{i0}+\phi_{o0})$, which yields coordinates for the orbiting scroll of

$$\left(x_o, y_o\right) = \left(-x_f + r_o\cos\theta_m, -y_f + r_o\sin\theta_m\right) \tag{2}$$

where the offset angle $\theta_m=\phi_{ie}-\theta+\pi/2$ is defined such that the suction chamber has zero volume at a crank angle θ of 0. The crank angle θ is defined to range between 0 and 2π which forms one revolution.

3. SUCTION CHAMBERS

The suction chamber defines how much mass will flow through the compressor, and as such is a critical component of the overall scroll compressor geometric analysis. In addition, the rate of change of the suction chamber volume will impact the thermodynamics of the suction process and can have an impact on the volumetric efficiency.

3.1 Suction Chamber Break Angle $\phi_{s\text{-}sa}$

As flow enters into the suction pocket from the suction port it first passes through a so called suction area, sometimes described as a suction plenum. The location of the angle which divides the suction chamber and the suction area is critical to a definition of the suction chamber volume. In addition this is the point around which the volume integration for the suction chamber will be carried out, so its precise location is critical to an accurate estimation of the suction chamber volume. This involute angle can be found by drawing a line from the base circle of the fixed scroll at a circle angle of ϕ_{ie} to the inner ending involute point on the fixed scroll, as shown in Figure 2, and finding the intersection involute angle $\phi_{s\text{-}sa}$. Equating the slope of the tangent of the base circle to the slope of the line from the point on the base circle to the involute angle $\phi_{s\text{-}sa}$ yields

$$\frac{dy}{dx} = \underbrace{\frac{-\cos\phi_{ie}}{\sin\phi_{ie}}}_{\substack{\text{Base}\\ \text{Circle}\\ \text{Tangent}}} = \underbrace{\frac{-\sin\phi_{s-sa} - \sin\phi_{ie} + (\phi_{s-sa} - \phi_{i0})\cos\phi - (\pi - \phi_{i0} + \phi_{o0})\cos(\phi_{ie} - \theta)}{-\cos\phi_{s-sa} - \cos\phi_{ie} - (\phi_{s-sa} - \phi_{i0})\sin\phi + (\pi - \phi_{i0} + \phi_{o0})\sin(\phi_{ie} - \theta)}}_{\text{Base Circle to } \phi_{s-sa}} \tag{3}$$

After simplification, the result is

$$\cos(\phi_{s-sa} - \phi_e) + (\phi_{s-sa} - \phi_{o0})\sin(\phi_{s-sa} - \phi_e) + (\pi - \phi_{i0} + \phi_{o0})\sin\theta = -1 \tag{4}$$

which does not offer a straightforward method of solution. From a consideration of the numerical solution, the following approximation for the suction chamber break angle was found:

$$\phi_{s-sa} = \frac{r_o / r_b}{\phi_e - \phi_{o0} - \pi}\sin\theta + \phi_e - \pi \tag{5}$$

Figure 3 shows the error in the approximate compared with the numerical solution of Eqn. 4. For the geometry investigated, the error in $\phi_{s\text{-}sa}$ is less than 0.01%, which motivates the further use of this high-accuracy approximation.

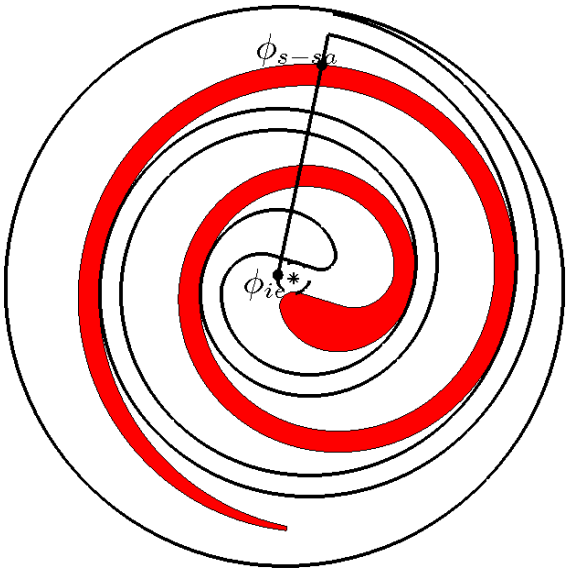

Figure 2 Scroll to obtain $\phi_{s\text{-}sa}$

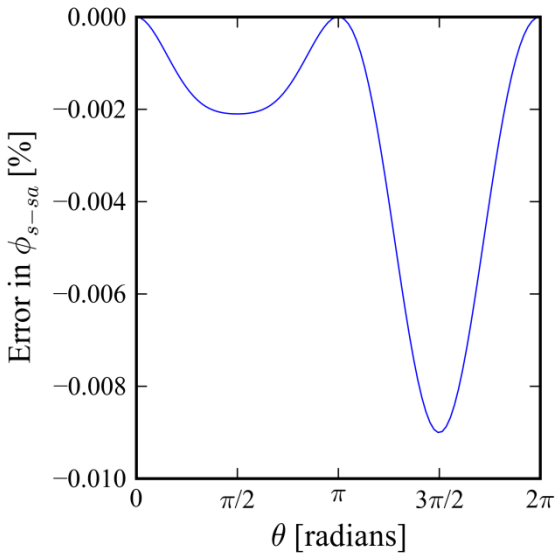

Figure 3 Error in approximate solution for $\phi_{s\text{-}sa}$

3.2 Suction chamber Geometry

The geometry of the suction pocket of the scroll compressor is complex. In Yanagisawa's formulation, the volume of the suction pocket is determined as the area integration based on the involute geometry, and a correction term is obtained which corrects for the intersection angle $\phi_{s\text{-}sa}$ described above. While Wang's solution is elegant and results in a compact form, shown in Eqn. 6 for reference, it is not analytically correct. Yanagisawa did not provide any details on how the correction term was derived, nor on what approximations were required to obtain this form. Attempts to re-derive this term based on various assumptions like the small angle assumption for perturbations around the mean angle were fruitless. Figures 4 to 7 show the correction term in action. The area in yellow is the area integration from the base circle which generates the fixed scroll involute to the fixed scroll, and the area in blue is the involute integration from the base circle which generates the orbiting scroll involute to the orbiting scroll. The area of the correction term is equal to the area that is either solid blue or solid yellow and not contained in the suction chamber.

$$V_{s-Wang} = \frac{h_s}{2} r_b r_o \left(2\theta\phi_e - \theta^2 - \theta\left(\phi_{i0} + \phi_{o0} + \pi\right) + 2\left(1 - \cos\theta\right) - 2\left(\phi_{ie} - \pi\right)\sin\theta - \frac{\pi}{4}\sin\left(2\theta\right) \right) \tag{6}$$

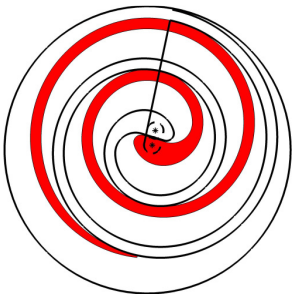

Figure 4 $\theta = 0$ (0°)

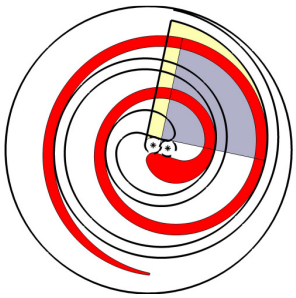

Figure 5 $\theta = \pi/2$ (90°)

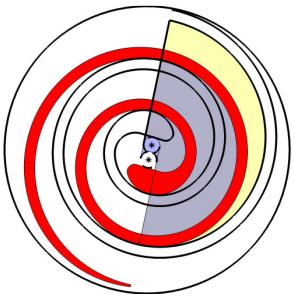

Figure 6 $\theta = \pi$ (180°)

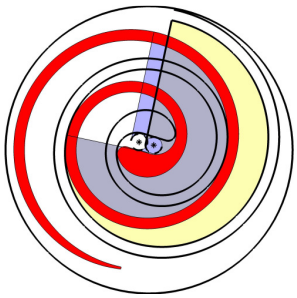

Figure 7 $\theta = 3\pi/2$ (270°)

A novel method is used here to arrive at a semi-analytic form for the suction chamber volume. The basis of this method is two polar integrations around the point on the inner scroll surface at the involute angle of $\phi_{s\text{-}sa}$. The primary challenge therefore is to arrive at a coordinate transformation from involute angle ϕ to polar integration angle α. As a convenient consequence of the mathematics involved in the polar integration, a relatively simple integrand is obtained.

The Cartesian coordinates of the point on the orbiting scroll with involute angle ϕ_{s-sa} for a given crank angle θ are given by

$$\begin{aligned} x_{s-sa} &= -r_b\left(\cos\phi_{s-sa} + \left(\phi_{s-sa} - \phi_{o0}\right)\sin\phi_{s-sa}\right) + r_o\cos\left(\phi_{ie} - \pi/2 - \theta\right) \\ y_{s-sa} &= -r_b\left(\sin\phi_{s-sa} - \left(\phi_{s-sa} - \phi_{o0}\right)\cos\phi_{s-sa}\right) + r_o\sin\left(\phi_{ie} - \pi/2 - \theta\right) \end{aligned} \tag{7}$$

and the coordinates of a point on the fixed and orbiting scrolls at an involute angle ϕ are given by

$$\begin{aligned} x_{orb} &= -r_b\left(\cos\phi + \left(\phi - \phi_{o0}\right)\sin\phi\right) + r_o\cos\left(\phi_{ie} - \pi/2 - \theta\right) \\ y_{orb} &= -r_b\left(\sin\phi - \left(\phi - \phi_{o0}\right)\cos\phi\right) + r_o\sin\left(\phi_{ie} - \pi/2 - \theta\right) \\ x_{fix} &= r_b\left(\cos\phi + \left(\phi - \phi_{o0}\right)\sin\phi\right) \\ y_{fix} &= r_b\left(\sin\phi - \left(\phi - \phi_{o0}\right)\cos\phi\right) \end{aligned} \tag{8}$$

For the fixed scroll's inner surface, which forms the outer part of the scroll chamber, the integration is taken around the point (x_{s-sa}, y_{s-sa}), where the integration angle α is defined by

$$\tan\alpha = \frac{\Delta y}{\Delta x} = \frac{r_b\sin\phi - r_b(\phi-\phi_0)\cos\phi - y_{s-sa}}{r_b\cos\phi + r_b(\phi-\phi_0)\sin\phi - x_{s-sa}} \tag{9}$$

This point is selected because the polar area integral around this point results in an integration without any double intersection of the integration ray and the involutes. Taking the arctangent of both sides of Equation 9 and then the derivative with respect to ϕ yields

$$\frac{\partial\alpha}{\partial\phi} = \frac{(\Delta x)^2}{R^2}\frac{\partial\tan\alpha}{\partial\phi} \tag{10}$$

and the differential area is given by:

$$dA = \frac{1}{2}R^2\underbrace{\frac{(\Delta x)^2}{R^2}\frac{r_b^2(\phi-\phi_0)^2 - r_b x_{s-sa}(\phi-\phi_0)\sin\phi + r_b y_{s-sa}(\phi-\phi_0)\cos\phi}{(\Delta x)^2}}_{d\alpha}d\phi \tag{11}$$

and the limits of integration for the inner fixed scroll involute are ϕ_{ie} to ϕ_{ie}-θ. A similar methodology is applied to the orbiting scroll for which limits of integration of ϕ_{s-sa} to ϕ_{ie}-θ-π are used. It should be noted that while the work of Blunier et al. (2006, 2009) derived analytic forms for the suction chamber volume, they have a different interpretation of the suction chamber volume, and they use the involute integration angles of ϕ_{ie}-π to ϕ_{ie}-θ-π for the orbiting scroll outer involute, which yields a different suction chamber volume evolution. For that reason, the results of Blunier are not compared here. The cross-sectional area of the suction chamber is then the area to the fixed scroll minus the area from the orbiting scroll. Finally the volume of the chamber can be found by multiplying by the scroll height. The result of a significant amount of algebra and trigonometric identity manipulations is the analytic form of the volume of the scroll chamber, given by

$$V_s = \frac{h_s r_b}{2}\cdot\begin{bmatrix} -r_o\theta(\pi - 2\phi_e + \phi_{i0} + \phi_{o0} + \theta) - r_b(\phi_e - \pi - \phi_{o0})^2 B \\ -r_b(\phi_e - \pi - \phi_{o0})B^2 - \frac{r_b}{3}B^3 \\ (\phi_e - \phi_{i0})(r_b\cos B + r_b\sin B(\phi_e - \pi + B - \phi_{o0}) - r_o\sin(\theta)) \\ +r_b\sin B - r_b\cos B(\phi_e - \pi + B - \phi_{o0}) - r_o\cos(\theta) \\ -r_o\sin(B+\theta)(\phi_e - \pi + B - \phi_{o0}) \\ -r_o\cos(B+\theta) + r_o \end{bmatrix} \tag{12}$$

where the term B is defined for compactness as

$$B = \frac{r_o / r_b}{\phi_e - \phi_{o0} - \pi} \tag{13}$$

Finally the derivative of the suction chamber volume is given by

$$\frac{dV_s}{d\theta} = \frac{h_s r_b}{2} \cdot \left[\begin{array}{l} -r_o(\pi - 2\phi_e + \phi_{i0} + \phi_{o0} + 2\theta) - r_o \cos\theta \left(C + B + \frac{1}{3}\frac{B^2}{C} \right) \\ (\phi_e - \phi_{i0}) \left(\frac{r_o \cos\theta}{C} [A\cos B - C] \right) + r_o \sin\theta \\ + r_o \cos\theta \left(\frac{A \sin B}{C} - A\cos(B+\theta)\frac{r_o / r_b}{C} \right) \\ + r_o(\sin(B+\theta) - A\cos(B+\theta)) \end{array} \right] \tag{14}$$

$$\begin{aligned} C &= (\phi_e - \pi - \phi_{o0}) \\ A &= C + B \end{aligned} \tag{15}$$

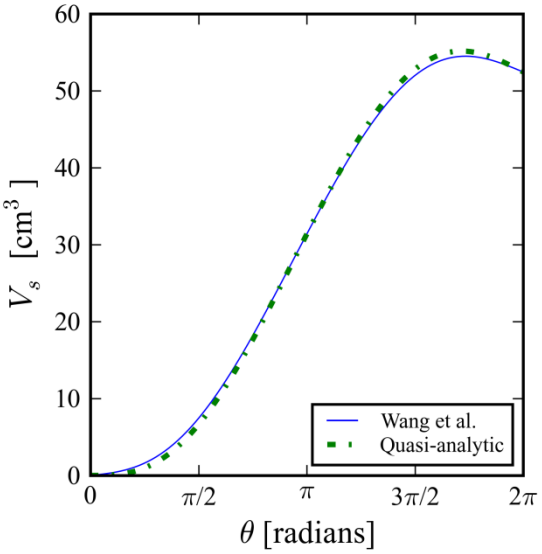

Figure 8 Volume of suction chamber

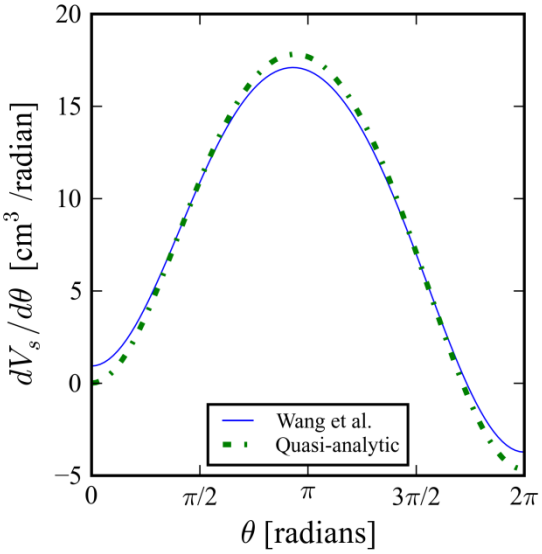

Figure 9 Differential of suction chamber volume

4. COMPRESSION CHAMBERS

Error! Reference source not found. Table 1 presents a comparison of the results from the analysis of Wang et al. (2005) and the current model with solutions based on area calculations of high accuracy polygons. This shows that the errors from the simplified Wang model are particularly significant at crank angles of π/2 and 3π/2, due to the error in the suction chamber correction term. The scroll compressor geometry of Bell et al. (2008) was used to generate the volumes.

Table 1 Suction chamber volumes evaluated from solutions of Wang and Bell

θ	V_s (Polygon) cm^3	V_s (Wang) cm^3	Error V_s (Wang) %	V_s (Bell) cm^3	Error V_s (Bell) %
π/2	6.627928	7.4307	12.11196	6.628928	0.015092
π	31.36861	31.36866	0.000157	31.36966	0.003345
3π/2	52.80177	51.99218	-1.53327	52.80297	0.00227
2π	52.44686	52.4472	0.000659	52.4482	0.002566

When the suction chamber volume expressions of Wang are implemented in a mechanistic scroll compressor model validated with high-accuracy polygon-based suction chamber volumes, the error in mass flow rate is up to 1 percent. Depending on the accuracy required, the simple expressions from Wang et al. (2005) may be sufficient. However,

when implemented into a full mechanistic model, the additional overhead from the solution presented here compared with the solution of Wang et al. (2005) is negligible.

The compression chambers have relatively simple geometry for which straight-forward analytic solutions are found. As an extension of Wang et al. (2005), the volume of the *k-th* compression chamber can be expressed as

$$V_{c,k} = -h_s r_b r_o \left(2\theta + 4\pi k - 2\phi_{ie} - \pi + \phi_{i0} + \phi_{o0}\right)$$
$$\frac{dV_{c,k}}{d\theta} = -2h_s r_b r_o \tag{16}$$

where the k=1 compression chamber is the outer-most chamber connected to the suction chamber. Thus this analysis allows for multiple compression chambers, which overcomes a limitation of the analysis of Wang et al. (2005) and others based on the same method.

5. DISCHARGE CHAMBERS

As shown previously in section 2**Error! Reference source not found.**, the involute portion of the scroll wraps terminates at the starting angle for both the inner and outer involutes. A set of curves are necessary to close the involute curves and obtain a scroll wrap which can be manufactured and has sufficient mechanical strength. Three potential solutions to the discharge geometry are the single arc, double arc and perfect meshing profile shown in Figure 10, Figure 11, and Figure 12 respectively, though other solutions are possible. The perfect meshing profile solution is commonly used in current scroll compressors. The single arc is not mechanically robust but simple to treat analytically. The two discharge arc solution can also be used, but is not very commonly applied. For that reason the analysis below focuses on the perfect-meshing-profile discharge geometry. The case of one discharge arc is a subset of the perfect-meshing-profile case. Analytic solutions for the perfect meshing profile (PMP) are found in Lee and Wu (1995). Alternatively, the PMP curves can be obtained from a graphical scan of the scroll, as was done here in order to obtain the parameters which define the arcs and line in the discharge region. The PMP is formed by three curves composed of two arcs and a single line.

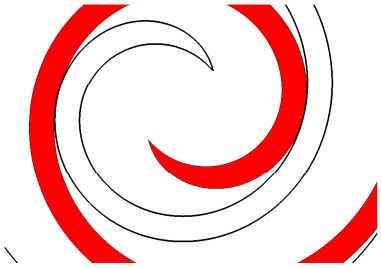

Figure 10 One Discharge Arc

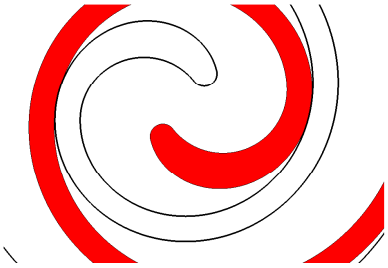

Figure 11 Two Discharge Arcs

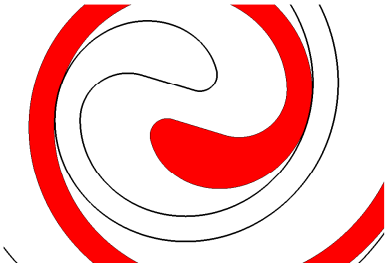

Figure 12 Perfect Meshing Profile

In order to calculate the volume of the discharge chamber, the discharge chamber is partitioned into a number of geometric regions, each of which has an analytic solution, and the total area is a combination of each of the regions. Figure 13 shows half of the discharge chamber with a perfect meshing profile. The total discharge chamber volume is twice that of the area shown. The critical point around which the integrals are carried out is the point labeled D, which has the coordinates:

$$\left(x_D, y_D\right) = \left(r_b\left(\cos\phi_{os} + \left(\phi_{os} - \phi_0\right)\sin\phi_{os}\right), r_b\left(\sin\phi_{os} - \left(\phi_{os} - \phi_0\right)\cos\phi_{os}\right)\right) \tag{17}$$

The areas ABD and DED are composed of an arc and lines. The polar integral can be taken around point D, sweeping out the entire region with one integral by the same method as for the suction chambers presented in section 2.

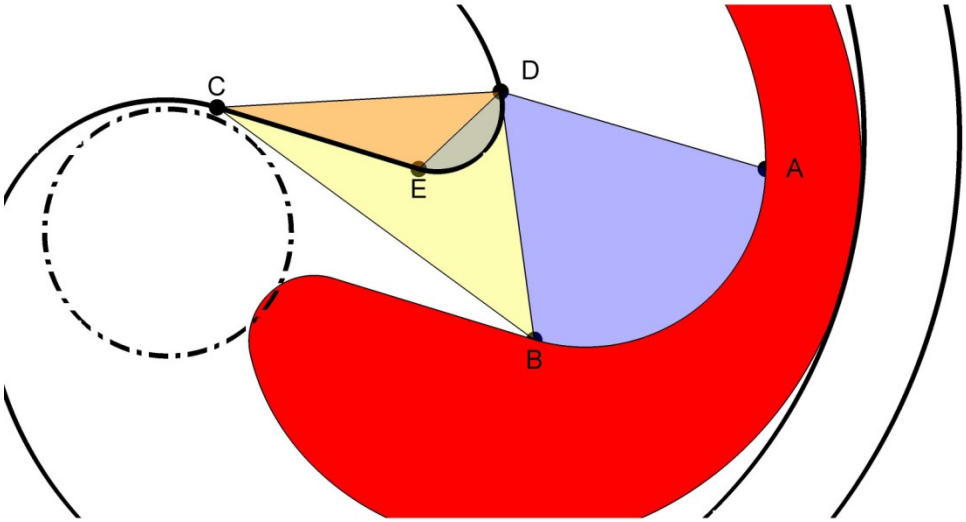

Figure 13 Discharge chamber geometry with perfect meshing profile

5.1 Area terms

In the analysis which follows for the discharge region, three different types of areas calculations are needed – the area of a triangle as well as the integral of an arc segment around a fixed point. In addition, the derivatives of the areas with respect to the crank angle are required. Table 2 shows the required equations. For the triangles, the line which forms the triangle is parameterized, and the same change of coordinates is applied in order to calculate the area.

Table 2 Equations for Discharge Geometry

Orbiting arc (ABD)	$A_{ABD} = \frac{r_a}{2}\left[r_a t + \sin t(x_{os} + x_a - r_o\cos\theta_m) - \cos t(y_{os} + y_a - r_o\sin\theta_m)\right]_{t_1}^{t_2}$ $\frac{dA_{ABD}}{d\theta} = \frac{-r_o r_a}{2}\left[\sin t\sin\theta_m + \cos t\cos\theta_m\right]_{t_1}^{t_2}$	(18)
Fixed arc (DED)	$A_{DED} = \frac{r_a}{2}\left[r_a t + \sin t(x_a - x_{os}) - \cos t(y_a - y_{os})\right]_{t_1}^{t_2}$ $\frac{dA_{DED}}{d\theta} = 0$	(19)
Triangle (CDE)	$A_{CDE} = \frac{1}{2}(-mx_{os} - b + y_{os})(t_2 - t_1)$ $\frac{dA_{CDE}}{d\theta} = 0$	(20)
Triangle (BCD)	$(x_D, y_D) = (x_{os}, y_{os})$ $(x_C, y_C) = (t, mt + b)$ $(x_B, y_B) = (-t + r_o\cos\theta_m, -mt - b + r_o\sin\theta_m)$ $A_{BCD} = -\frac{1}{2}\left[(x_B - x_D)(y_C - y_D) - (x_C - x_D)(y_B - y_D)\right]$ $\frac{dA_{BCD}}{d\theta} = -\frac{1}{2}\left[r_o\sin\theta_m(y_C - y_D) + r_o\cos\theta_m(x_C - x_D)\right]$	(21)

The volume of the discharge chamber and its derivative with respect to the crank angle can be obtained through the appropriate combination of the segment areas, multiplied by the scroll height. The terms are doubled since the areas calculated above compose only one half of the discharge chamber cross-section.

$$V_{dd} = 2h_s\left(A_{ABD} + A_{BCD} - A_{DED} - A_{CDE}\right)$$
$$\frac{dV_{dd}}{d\theta} = 2h_s\left(\frac{dA_{ABD}}{d\theta} + \frac{dA_{BCD}}{d\theta} - \frac{dA_{DED}}{d\theta} - \frac{dA_{CDE}}{d\theta}\right) \quad (22)$$

CONCLUSIONS

Novel approaches were presented for the calculation of the chamber volumes of the scroll compressor that can be applied to the suction, compression, and discharge chambers. The solution yields excellent agreement with high-accuracy polygon solutions and overcomes several limitations of earlier approaches, including improved solutions for the suction chamber geometry, the novel ability to handle multiple compression chambers, and calculations of analytic solutions to the perfect-meshing-profile discharge geometry.

NOMENCLATURE

Variable	Definition (Units)	Subscript	Description
A	Area (m^2)	a	Arc
α	Polar Integration Angle (rad)	b	Base circle
b	Intercept of line (m)	c	Compression
ϕ	Involute Angle (rad)	dd	Discharge Region
h_s	Height of Scroll (m)	f	Fixed Scroll
k	Compress. Chamber Index (-)	i0	Inner Initial
m	Slope of line (-)	is	Inner Starting
r	Radius (m)	ie	Inner Ending
t	Parametric Parameter (-)	o0	Outer Initial
θ_m	Offset Angle (rad)	os	Outer Starting
θ	Shaft Crank Angle (rad)	oe	Outer Ending
x	x Cartesian Coordinate (m)	o	Orbiting
y	y Cartesian Coordinate (m)	s	Suction
V	Volume (m^3)	0	Initial

REFERENCES

Bell, I., Lemort, V., Braun, J. & Groll, E., 2008, Development of liquid-flooded scroll compressor and expander models, *19th International Compressor Engineering Conference at Purdue University*, number 1283.

Blunier, B., Cirrincione, G. & Mairaoui, A., 2006, Novel Geometrical Model of Scroll Compressors for the Analytical description of the chamber volumes, *2006 International Compressor Engineering Conference at Purdue University*

Blunier, B., Cirrincione, G., Hervé, Y. & Miraoui, A., 2009, A new analytical and dynamical model of a scroll compressor with experimental validation, *Int. J. Refrig.*, Vol. 32, pp. 874-891

Chen, Y., Halm, N., Groll, E. & Braun, J., 2002, Mathematical Modeling of Scroll Compressor Part I- Compression Process Modeling, *Int. J. Refrig.*, Vol. 25, pp. 731-750

Gravesen, J. & Henriksen, C., 2001, The Geometry of the Scroll Compressor, *Society for Industrial and Applied Mathematics*, Vol. 43, pp. 113-126

Halm, N., 1997, Mathematical Modeling of Scroll Compressors, Masters Thesis Purdue University

Lee, Y., & Wu, W., 1995. On the profile design of a scroll compressor, *Int. J. Refrig.*, Vol. 18, No. 15, pp. 308-317

Wang, B., Li, X. & Shi, W., 2005, A general geometrical model of scroll compressors based on discretional initial angles of involute, *Int. J. Refrig.*, Vol. 28, pp. 958-966

Yanagisawa, T., Cheng, M.C., Fukuta, M. & Shimizu, T., 1990, Optimum Operating Pressure Ratio for Scroll Compressor, *1990 International Compressor Engineering Conference at Purdue University*